

Enumeration, Nomenclature and Stability

Rules of Carbon Nanobelts

Yang Wang,* Yi Zhou, and Ke Du

School of Chemistry and Chemical Engineering, Yangzhou University, Yangzhou, Jiangsu 225002, China

E-mail: yangwang@yzu.edu.cn

Abstract

With the recent breakthroughs and advances in synthetic chemistry, carbon nanobelts (CNBs) have become an emerging hot spot in chemistry and materials science. Owing to their unique molecular structures, CNBs have intriguing properties with applications in synthetic materials, host–guest chemistry, optoelectronics, and so on. Although a considerable number of CNBs with diverse forms have been synthesized to date, no systematic nomenclature is available yet for this important family of macrocycles. Moreover, little is known about the detailed isomerism of CNBs, which, in fact, exhibits greater complexity than that of carbon nanotubes. The copious variety of CNB isomers, along with the underlying structure–property relationships, bears fundamental relevance to the ongoing design and synthesis of novel nanobelts. In this paper, we propose an elegant approach to systematically enumerate, classify, and name all possible isomers of CNBs. Besides the simplest, standard CNBs defined by chiral indices (n, m) , the nonstandard CNBs (n, m, l) involves an additional winding index l . Based on extensive quantum chemical calculations, we present a comprehensive study of the relative isomer stability of CNBs containing up to 30 rings. A simple Hückel-based model with a high predictive power reveals that the relative stability of standard CNBs is governed by the π stabilization and the strain destabilization induced by cylindrical carbon framework, and the former effect prevails the latter. For nonstandard CNBs, a third stability factor, the H...H repulsion in the benzo[c]phenanthrene-like motifs, is shown to be also important and can be incorporated into the simple quantitative model. In general, lower-energy CNB isomers have a larger HOMO–LUMO gap, suggesting that their thermodynamic stability coincides with kinetic stability. The determined most stable CNB isomers can be considered as the optimal targets for future synthesis. These results lay an initial foundation and provide a useful theoretical tool for further research on CNBs and related analogs.

1 Introduction

Carbon nanobelts (CNBs) are an intriguing family of aromatic macrocyclic hydrocarbons that have been recently receiving an escalating attention in the chemical community.^{1–5} Structurally, they can be regarded as sidewall cutouts of carbon nanotubes (CNTs) and are conventionally defined as closed molecular loops consisting solely of fully unsaturated and fused benzene rings. Compared with the analogous carbon nanorings (CNRs),^{1,5–7} for a CNB we need to break at least two C—C bonds to open its macrocyclic framework whereas the cleavage of only one bond is required in the CNR case.^{4,8} As a more strict definition, CNBs are considered by many chemists as double-stranded structures with a single layer of benzene rings,^{3,5,7,9–15} although multilayered nanobelts, such as the Vögtle belt,^{16,17} are also frequently known.^{13,18,19}

Due to their cylindrical carbon skeleton, CNBs are highly strained molecules and first-principles calculations^{20,21} have shown that they are generally higher in energy than the macrocyclic topoisomers of other types, like the generalized kekulenes,^{20–22} clarenes^{20,21} and even the doubly-twisted, infinitene²³ and its generalized analogs.^{20,24,25} Nevertheless, because of their aesthetically pleasing structures, CNBs have become a long-standing synthetic target for ambitious chemists since the first CNB molecule, [n]cyclacene, was theoretically conceived in 1954.²⁶ Over the past six decades, a great deal of efforts by generations of synthetic chemists had been devoted to the synthesis of these challenging compounds, but all attempts were unsuccessful. In 2011, the formation of an armchair CNB, [10]cyclophenacene, was observed by laser desorption ionization time-of-flight mass spectroscopy, though the attempted isolation of the product proved futile.²⁷ The first genuine CNB was synthesized and isolated by Itami et al. in 2017²⁸ and has now become a commercially available product.²⁹ Since this milestone achievement, ten more CNBs of different types and sizes have been successfully synthesized by various teams.^{12,13,18,19,30,31} Thanks to the recent synthetic advancements and the high fundamental and practical significance of these fascinating molecules, CNBs have currently become a burgeoning research area in chemistry and materials science.^{2,4}

The distinctive structures of CNBs endow them with unique properties and potential applications in electronics, photonics, and optoelectronics. First, CNBs have been proposed as molecular seeds or templates for the bottom-up precise synthesis of uniform, single-chirality CNTs, which is regarded as one of the ultimate goals in CNT industry.^{4,5} As another application in synthetic chemistry, CNBs can be exploited as building blocks for making more complex nanocarbon architectures,⁴ as exemplified by the synthesis of cycloptycenes from CNBs.³² On the other hand, the electron-rich macrocyclic framework of CNBs makes them ideal hosts to selectively capture guest molecules.¹¹ In turn, CNBs can be inserted inside larger nanoporous materials as well. In a recent experiment, an antiaromatic metal–organic framework caused a substantial downfield shifting in the ¹H nuclear magnetic resonance signals of the encapsulated CNB.³³ These host–guest examples involving CNBs suggest interesting implications in molecular recognition and supramolecular self-assembly.¹¹ Moreover, owing to their double-stranded cylindrical skeleton, the radial π-conjugation in CNBs brings about more efficient orbital overlaps than the linear conjugation. As a result, CNBs are supposed to have remarkable charge transport properties¹⁵ and be generally more conductive than linear conjugated semiconductors,⁵ which was confirmed by both experimental¹⁴ and computational studies.³⁴ Lastly, photophysical measurements^{13,30} and excited state simulations^{35,36} demonstrated that CNBs exhibit peculiar photophysical and fluorescent properties and, as envisioned in ref. 35, we could make use of the supramolecular chemistry of CNBs to modulate these properties by varying the guest species.

In light of the increasing importance of the CNB chemistry, we propose here a systematic approach to the enumeration and nomenclature of CNBs of all types and sizes, which we believe is of urgent significance to the emerging nanobelt science and technology. Although a considerable number of CNB molecules with various types and sizes have been synthesized and identified, not to mention the numerous synthesized CNB analogs (e.g., partially saturated, heteroatom-embedded),^{2,4,5} there has not yet been a systematic naming system established for this significant class of macrocycles, to the best of our knowledge. This is not

a trivial matter. The structures of CNBs are actually more complex than those of CNTs, since, given a fixed CNT structure, there are usually a plethora of possible ways to cut out a valid CNB segment, which brings an additional dimension to the structural description. As we will see in the following section, the number of possible isomers of CNBs increases exponentially as the CNB size enlarges. For example, the single-walled armchair CNT (6, 6) has only one structure, but there exist 35 distinct molecular structures for CNBs (6, 6) and this number explodes to nearly thirty thousand for the double-sized CNBs (12, 12).

Furthermore, as the synthetic technique further advances, we can anticipate a growing number of forthcoming CNB structures with a greater variety of types and sizes, thus offering a diversified properties and functions to promote the applications of CNB-related materials. For instance, comparative experimental measurements combined with density functional theory (DFT) calculations discerned that three CNBs of the same (armchair) type but different sizes exhibited diverse characteristics in the fluorescence spectra, as a consequence of the size-dependent energy shifts of their frontier orbitals.³⁰ Therefore, it would be valuable to predetermine the energetically favorable isomers, among a vast number possibilities, as promising candidates for future synthesis and applications. More importantly, since the properties of CNTs depend strongly on their chirality, a curious fundamental question is how the stability of CNBs is connected with their chirality and/or other structural characteristics. In this work, we carry out exhaustive quantum chemical computations of an enormous number of CNB structures, covering a wide range of chiralities and sizes. We present a comprehensive theoretical investigation on the relative stability of CNB isomers and uncover the determining stability factors. The derived simple topology-based models allow us to quantitatively predict with high confidence the relative isomer stability for CNBs. The simple stability rules and models, coupled with strategic searches, have eventually unveiled the CNB structures with the highest stability as the optimal targets for upcoming synthetic studies.

2 Enumeration and Nomenclature of CNB Structures

In this work, we consider systematically the single-layered CNBs, a prototypical type of aromatic hydrocarbon belts that consist of cata-condensed³⁷ benzene rings, forming a double strand of carbon atoms (see ref. 28,30 for recent synthetic examples). On the other hand, a multilayered nanobelt possesses additional benzene rings attached to essential belt structure,^{18,31} and may also contain peri-condensed³⁷ rings.^{13,18,19} For brevity, hereafter we refer to the double-stranded CNBs simply as CNBs, i.e., following the more strict definition.^{3,5,7,9–15}

2.1 Chirality of CNBs and Their Connection to CNTs

As shown in the right panel of Figure 1a, a CNB structure can be regarded as cut out from a single-walled CNT structure, which is uniquely defined by a pair of integer indices (n, m) for chirality.^{38–41} It has been well recognized that CNTs are categorized into three structural types depending on the chiral indices: the armchair type when $n = m > 0$, the zigzag type when one of the indices is zero, and the chiral type for the rest of cases. For the zigzag and chiral types, conventionally, we need only to consider the right-handed CNT (n, m) with $n > m \geq 0$, which is symmetrically equivalent to the left-handed CNT (n, m) where $m > n \geq 0$.⁴¹ The 3D structure of CNT (n, m) can be obtained by rolling up a 2D graphene sheet along the curl vector, $\vec{C} = n\vec{a} + m\vec{b}$ (\vec{a} and \vec{b} being the lattice vectors of graphene), as illustrated in Figure 1a. The translation vector, $\vec{T} = n'\vec{a} + m'\vec{b}$, which is perpendicular to \vec{C} , becomes the periodic (axial) direction of the resultant CNT. Accordingly, CNB structures have usually been designated the same chiral indices (n, m) as those for the CNTs where the CNBs are cut out from.^{1,3–5,18,30} Figure 1a demonstrates the construction of CNB $(7, 0)$ (represented by green rings) by rolling up the graphene nanosheet along the horizontal direction, $\vec{C} = OC = 7\vec{a}$.

Generally speaking, however, there may exist more than one way to cut out a CNB segment from the sidewall of CNT of the same chirality (n, m) . For instance, we can find

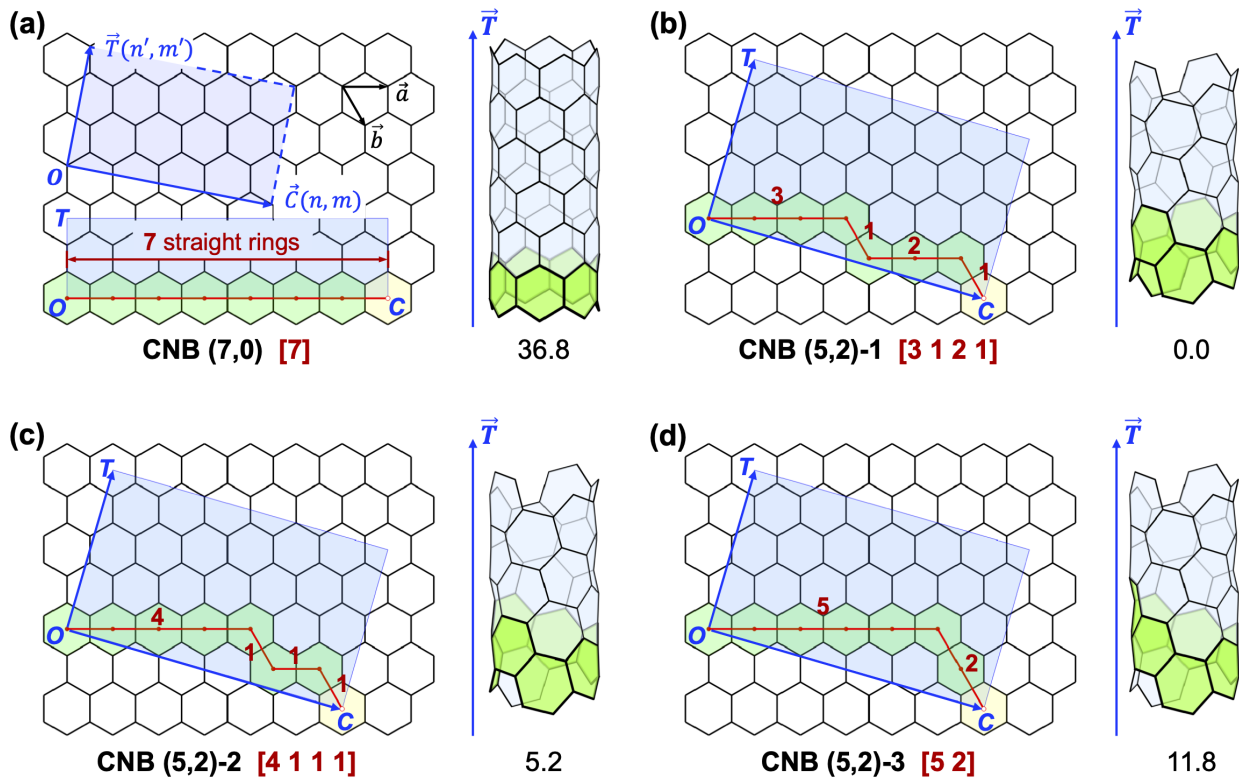


Figure 1. Schematic explanation of nomenclature and construction of CNB isomers with different chiralities and circular paths for (a) CNB (7,0), (b) CNB (5,2)-1, (c) CNB (5,2)-2, and (d) CNB (5,2)-3. The path code of each of the CNBs is given in square brackets. The curl vector, \vec{C} , and the translation vector, \vec{T} are indicated by blue arrows and are defined by coordinates (n, m) and (n', m') , respectively, in terms of the basic vectors, \vec{a} , and \vec{b} , of 2D graphene lattice. The CNT unit cell determined by \vec{C} and \vec{T} is represented by a light blue box. Each CNB structure (highlighted as green rings) unfolded onto 2D graphene nanosheet is defined by the associated CNT chirality (n, m) and the path (indicated by dark red lines) running through the centers of rings of the CNB. The lengths of path segments are indicated beside the path. Rolling up the 2D unfolded structure along the corresponding curl vector, we obtain the 3D CNB structure (green rings only) shown in the right panel of each subfigure. The DFT computed relatively energies among these [7]CNB isomers are provided in kcal/mol.

three different ways to construct CNBs (5,2) with 7 rings, as depicted in Figure 1b-d. The number of possible CNB isomers increases drastically with the increasing size of the nanobelt. For example, there are nearly thirty thousand isomers for CNBs (12,12) with 24 rings (see Table S1 in Supporting Information). Moreover, it is also possible to make CNBs (n, m) with more than $n + m$ rings, which have been found in the recently synthesized zigzag-type CNBs, whose essential belt structures were identified as two different (16,0) CNBs with 20

rings and a $(24, 0)$ CNB with 30 rings.¹² Thus, if such kind of CNBs is allowed to take into account, one needs to introduce an additional *winding index*, l , to the chiral indices (n, m) , as will be discussed in detail below. Let us refer to the CNBs (n, m) with $n + m$ ring as *standard CNBs* and call the CNBs (n, m, l) with $n + m + l$ rings *nonstandard CNBs*.

To cut a single-layered CNB segment from the sidewall of CNT (n, m) (see Figure 1b for example), we choose a strip of rings that starts from the one centered at the origin O and ends at the one centered at point C (the yellow ring in Figure 1b), as given by the curl vector \vec{C} . When we roll up the whole strip of rings along \vec{C} to make a looped nanobelt, we exclude the last ring C because it is circularly equivalent to the starting ring O . This procedure can be mathematically described as choosing a directional path starting from the origin point O to the ending point C , with each of the CNB rings represented by a node in the path (see the dark red lines in Figure 1b). Let such a path for making a CNB structure be denominated the *construction path* of the CNB. For the sake of convenience, we refer to each pair of adjacent nodes as a *step* in the construction path. We define the k th *step vector*, \vec{s}_k , as the vector from the $(k - 1)$ th node to the k th node in the path and $k = 0$ corresponds to the starting point O . Evidently, the sum of all step vectors equals the curl vector:

$$\sum_{k=1}^{\text{NR}} \vec{s}_k = \vec{C} = n\vec{a} + m\vec{b} \quad (1)$$

where NR is the number of rings in the CNB, since the number of steps is equal to the number of nodes in the circular construction path.

2.2 Construction and Enumeration of Standard CNBs (n, m)

We first explain the algorithm to construct and enumerate all possible isomeric structures of the standard CNBs (n, m) , which are the forms of most of the CNBs synthesized so far^{13,18,19,28,30,31} (see Figure 2). As the simplest type of nanobelts, the standard CNBs are constructed by following the shortest construction paths. That is, for any given chirality

(n, m) , the shortest paths between points O and C generate the CNBs with a minimum possible number of rings, resulting in the standard CNBs containing $n + m$ rings, which can be rationalized as follows.

As shown in Figure 1, since the starting point of the construction path, O , lies at the leftmost and topmost position relative to the ending point, C , all step vectors must be either the basic vector \vec{a} or \vec{b} so as to make the whole path as short as possible. Any other option for step vectors (e.g., $\vec{a} - \vec{b}$ or $-\vec{b}$) involves going leftward or upward and thus makes the path from O to C inevitably longer than the shortest one. It follows that any possible shortest path going from O to C consists exactly of n vectors of \vec{a} and m vectors of \vec{b} , and the only difference between two distinct shortest paths lies in the ordering of these n \vec{a} and m \vec{b} vectors. As the number of rings of a standard CNB (n, m) equals the total number of basic vectors constituting the whole path, we obtain from Equation 1 that

$$\text{NR} = n + m \quad (2)$$

To identify the ordering of basic vectors in a given path, we divide the path into a series of *path segments*, each consisting of only \vec{a} or only \vec{b} as step vectors. In other words, each segment corresponds to a maximum number of linearly arranged benzene rings. The nodes that connect adjacent segments are called *turning points* in the construction path. For instance, for the CNB (5,2) isomer shown in Figure 1b, the corresponding shortest path, as going from O to C , is split into three segments, which are composed, consecutively, of 3 \vec{a} , 1 \vec{b} , 2 \vec{a} , and 1 \vec{b} vectors. We may therefore conveniently assign a *path code*, [3 1 2 1], to this particular isomer of CNB (5,2) in Figure 1b. As we can see, there are four turning points in the construction path of this isomer (including the starting point O because of the circular boundary condition). Likewise, the other two isomers of CNB (5,2) shown in Figures 1c,d can be encoded as [4 1 1 1] (with 4 turning points) and [5 2] (with 2 turning points), respectively.

In general, a CNB (n, m) structure built following a shortest path is identified using a path code consisting of an even number (τ) of positive integers, $n_1, m_1, n_2, m_2, \dots, n_{\tau/2}, m_{\tau/2}$, where τ is the number of turning points (nodes) in the path. While $n_1, n_2, \dots, n_{\tau/2}$ represent, consecutively, the lengths of the path segments made of \vec{a} vectors along the path, $m_1, m_2, \dots, m_{\tau/2}$ correspond to the lengths of the path segments following \vec{b} vectors. As a result, using Equation 1, it is readily to establish that

$$\sum_{i=1}^{\tau/2} n_i = n \quad (3)$$

$$\sum_{i=1}^{\tau/2} m_i = m \quad (4)$$

For the special case of zigzag CNBs $(n, 0)$ (i.e., $m = 0$), there is only one possible shortest path with a unique path code of $[n]$, as it has no turning points ($\tau = 0$) and consists of only horizontal step vectors ($\vec{C} = n\vec{a}$), as exemplified by CNB $(7, 0)$ shown in Figure 1a.

As such, we can nicely convert the problem of enumerating CNB structures into a pure mathematical problem of integer partition and combinatorial arrangements of the parts. The basic idea is as follows. Given a pair of positive⁴² integers, n and m , we look for all possible ways of partitioning n into a varying number of positive integers, $n_1, n_2, \dots, n_{\tau/2}$, and all partitions of m with the *same* number ($\tau/2$) of partitions, $m_1, m_2, \dots, m_{\tau/2}$. Subsequently, we combine alternately the two sets of parts, $n_1, n_2, \dots, n_{\tau/2}$ and $m_1, m_2, \dots, m_{\tau/2}$, and then enumerate all nonequivalent combinations and orderings of these τ numbers. To be more specific, we generate all partitions of n (and of m) using the ascending composition generation algorithm.⁴³ Then, we enumerate all unique permutations of the parts of n and those of m , which are order-dependent and are termed as the *compositions* of n and m in the terminology of number theory and combinatorics. By putting together each part of each composition of n and each part of each composition of m in an alternate manner, we get a sequence of path code, namely, $n_1, m_1, n_2, m_2, \dots, n_{\tau/2}, m_{\tau/2}$, as a possible combination that corresponds to each of the possible isomers of CNB (n, m) . Note that we only combine the parts of n and of

m with the same number of partitions, i.e., $\tau/2$. After removal of all duplicated path codes, we end up with all nonequivalent path codes, each of which represents uniquely a possible construction path and therefore a unique isomer of CNBs (n, m) .

It is worth providing more details on determining equivalent path codes in order to eliminate the duplicated ones. The key is to find a *canonical path code* of a given path code according to the following procedure. We circularly shift (both clockwise and counterclockwise) the numbers in a path code to generate all circularly equivalent path codes, among which we choose the one with lexicographically largest numbers as the canonical path code. For example, we determine the canonical path code of [2 1 1 2 3 1] to be [3 2 1 1 2 1] by reversing and/or circularly shifting the original path code so that the largest numbers in the code sequence appear as early as possible. Given a set of path codes, we can thus obtain all unique ones by comparing their canonical path codes. In passing, the enumeration of all shortest paths is much more efficient if we combine all compositions of m with all *nonequivalent* compositions of n .

Table 1 lists the numbers of all possible isomers of standard CNBs of all possible chiralities with no more than 16 rings. As we can see, there exist only one possible structure for zigzag CNBs $(n, 0)$ and for CNBs $(n, 1)$. For CNBs $(n, 2)$, the number of isomers can be calculated as $[n/2] + 1$, where $[]$ is the floor function for rounding a number down to its nearest integer. We can also see that, given the same number of rings, the number of isomers increases as n and m become closer to each other. The only exception is that armchair CNBs (n, n) has fewer isomers than CNBs $(n + 1, n - 1)$, because of the higher symmetry of the armchair belts.

2.3 Nomenclature of Standard CNBs

The canonical path codes enable a systematic numbering of all isomers of the standard CNBs (n, m) . We sort all isomers using the following rules: (i) the isomers with a larger number of turning points in the construction path (i.e., a larger τ) appear earlier in the ordered list;

Table 1. Number of isomers (N_{iso}) of standard CNBs of chirality (n, m) with the number of rings (NR) ranging from 3 to 16.

NR	(n, m)	N_{iso}	NR	(n, m)	N_{iso}	NR	(n, m)	N_{iso}
3	(3, 0)	1	10	(10, 0)	1	14	(14, 0)	1
	(2, 1)	1		(9, 1)	1		(13, 1)	1
4	(4, 0)	1	11	(8, 2)	5	15	(12, 2)	7
	(3, 1)	1		(7, 3)	8		(11, 3)	16
	(2, 2)	2		(6, 4)	16		(10, 4)	47
5	(5, 0)	1	12	(5, 5)	13	16	(9, 5)	79
	(4, 1)	1		(11, 0)	1		(8, 6)	126
	(3, 2)	2		(10, 1)	1		(7, 7)	85
6	(6, 0)	1	13	(9, 2)	5	17	(15, 0)	1
	(5, 1)	1		(8, 3)	10		(14, 1)	1
	(4, 2)	3		(7, 4)	20		(13, 2)	7
	(3, 3)	3		(6, 5)	26		(12, 3)	19
7	(7, 0)	1	14	(12, 0)	1	18	(11, 4)	56
	(6, 1)	1		(11, 1)	1		(10, 5)	111
	(5, 2)	3		(10, 2)	6		(9, 6)	185
	(4, 3)	4		(9, 3)	12		(8, 7)	232
8	(8, 0)	1	15	(8, 4)	29	19	(16, 0)	1
	(7, 1)	1		(7, 5)	38		(15, 1)	1
	(6, 2)	4		(6, 6)	35		(14, 2)	8
	(5, 3)	5		(13, 0)	1		(13, 3)	21
	(4, 4)	7		(12, 1)	1		(12, 4)	72
9	(9, 0)	1	16	(11, 2)	6	20	(11, 5)	147
	(8, 1)	1		(10, 3)	14		(10, 6)	280
	(7, 2)	4		(9, 4)	35		(9, 7)	375
	(6, 3)	7		(8, 5)	57		(8, 8)	257
	(5, 4)	10		(7, 6)	76			

(ii) those with the same value of τ are sorted lexicographically in ascending order of their canonical path codes. As a result, we can assign the ranking numbers in the sorted list of canonical path codes to the CNB isomers in their nomenclature. For example, the ordering of the canonical path codes for the three isomers of CNBs (5, 2) in Figure 1b–d complies

with rule (i): [3 1 2 1], [4 1 1 1], and [5 2]. Accordingly, these isomers are named (5, 2)-1, (5, 2)-2, and (5, 2)-3, respectively. Now, we are able to provide systematic names for most of the CNBs that have been synthesized, as summarized in Figure 2. Note that in some cases a few side rings (colored in pink) are appended to the macrocyclic structure, but the essential belt structure (the green rings) can be unequivocally identified using our naming system.

2.4 Enumeration and Nomenclature of Nonstandard CNBs (n, m, l)

Now, we extend the standard CNBs (n, m) to the nonstandard CNBs (n, m, l) by allowing an additional basic vector $\vec{b}' = \vec{a} - \vec{b}$ (see Figure 3a) to constitute the step vectors in the construction path. Thus, the whole construction path for a nonstandard CNB (n, m, l) consists of N path segments of horizontal steps of \vec{a} vectors, M segments of downward and rightward steps of \vec{b} , and L segments of upward and rightward steps of \vec{b}' . Enumerating all nonequivalent combinations and orderings of these path segments of three types of steps, we obtain all possible isomers of nonstandard CNBs (n, m, l).

As the path goes from the origin O to C , we have the following relationship between the basic vectors (cf. Equation 1):

$$\sum_{i=1}^N n_i \vec{a} + \sum_{i=1}^M m_i \vec{b} + \sum_{i=1}^L l_i \vec{b}' = n \vec{a} + m \vec{b} \quad (5)$$

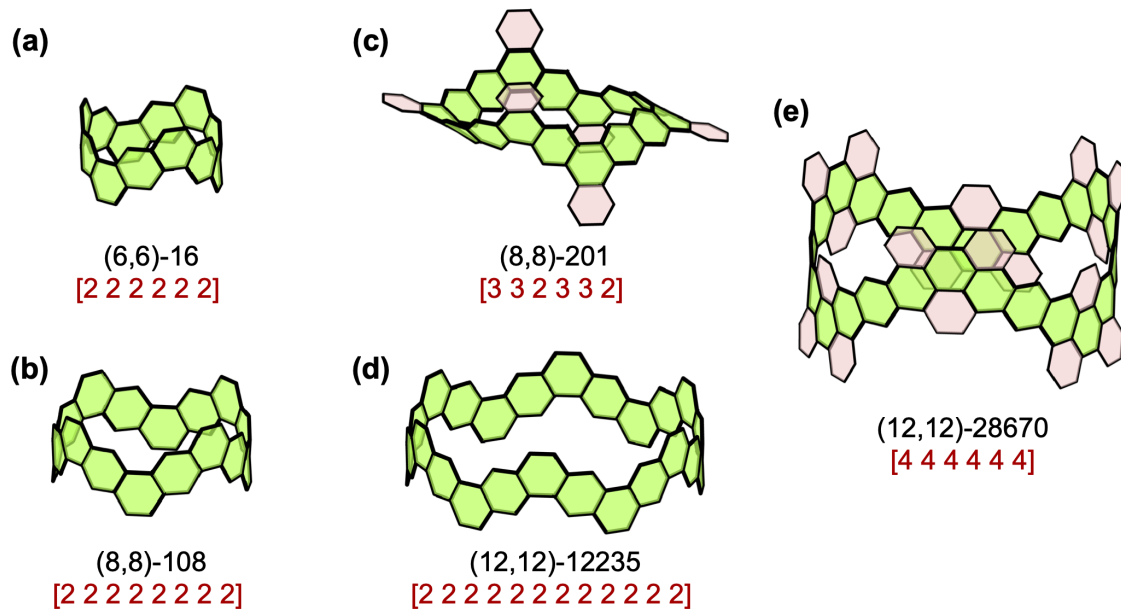
Knowing that $\vec{b}' = \vec{a} - \vec{b}$, we obtain from the above equation

$$n = \sum_{i=1}^N n_i + \sum_{i=1}^L l_i \quad (6)$$

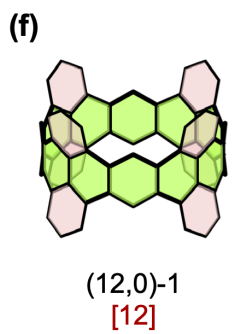
$$m = \sum_{i=1}^M m_i - \sum_{i=1}^L l_i \quad (7)$$

We define l as the total number of basic vectors \vec{b}' constituting the entire path, and conse-

Armchair Type:



Zigzag Type:



Chiral Type:

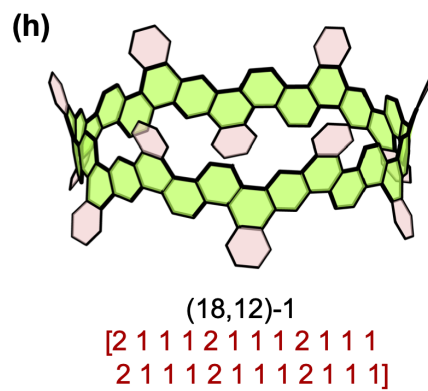


Figure 2. Representative synthesized CNBs of different chiralities and sizes, including the armchair CNBs (a) (6,6)-16,^{28,30} (b) (8,8)-108,³⁰ (c) (8,8)-201,³¹ (d) (12,12)-12235,³⁰ (e) (12,12)-28670,¹⁸ the zigzag CNBs (f) (12,0)-1,¹³ (g) (18,0)-1,¹⁹ and the chiral CNB (h) (18,12)-1.¹⁸ The canonical path codes are given in square brackets for each CNB. Green rings indicate those comprising the single-layered CNB structure, while the side rings are colored in pink. All hydrogens and/or substituent groups are omitted for clarity.

quently

$$l = \sum_{i=1}^L l_i \quad (8)$$

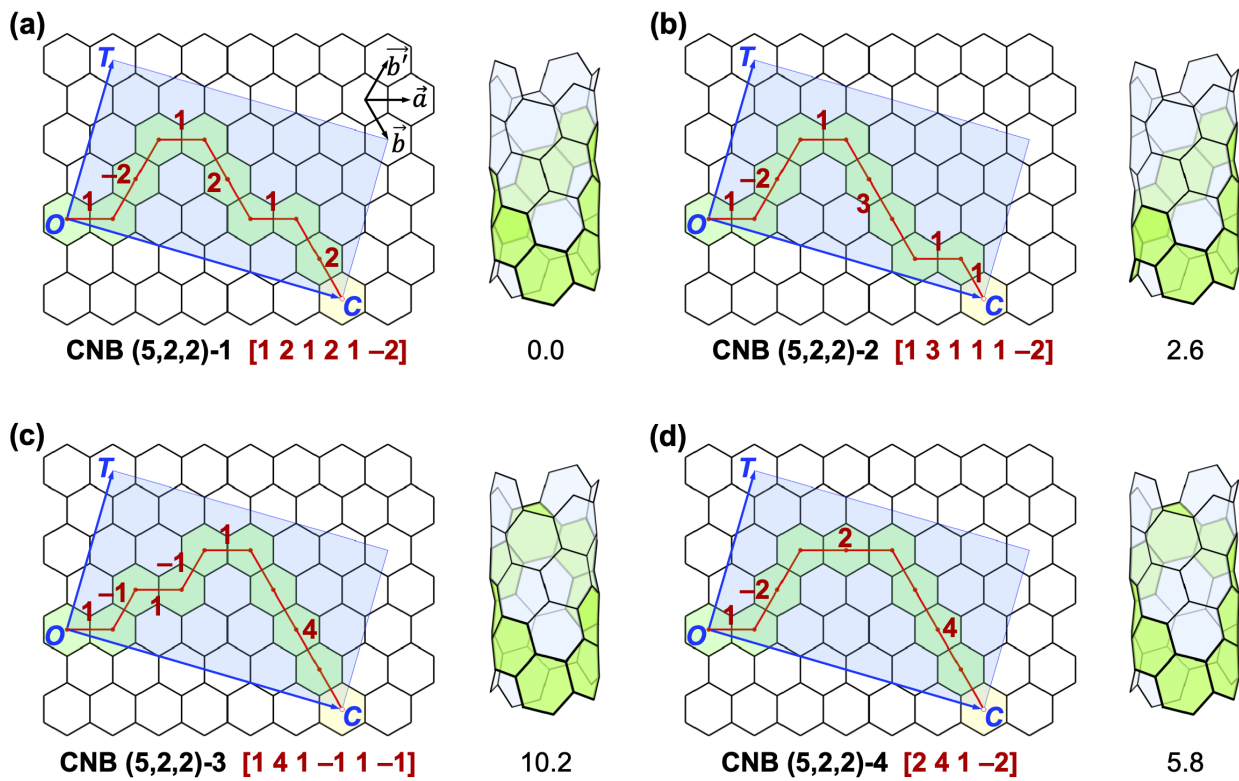


Figure 3. Schematic explanation of nomenclature and construction of the nonstandard CNB isomers (a) (5, 2, 2)-1, (b) (5, 2, 2)-2, (c) (5, 2, 2)-3, and (d) (5, 2, 2)-4. The canonical path code of each of the CNBs is provided in square brackets. The CNT unit cell determined by \vec{C} and \vec{T} is depicted as a light blue box. The three types of basic vectors, \vec{a} , \vec{b} , and \vec{b}' , that constitute the construction path are indicated by black arrows in (a). Each CNB structure (highlighted as green rings) unfolded onto graphene nanosheet is determined by the path (indicated by dark red lines) passing through the centers of rings of the CNB. The lengths of path segments are indicated beside the path. For better visualization, the actual illustrated paths follow circularly shifted but equivalent path codes. In the right panel of each subfigure, the corresponding 3D structure (green rings only) of each isomer is depicted, along with their DFT relatively energies indicated in kcal/mol.

According to Equations 6–8, let us define two new, positive integers, \tilde{n} and \tilde{m} , as

$$\tilde{n} = n - l = \sum_{i=1}^N n_i \quad (9)$$

$$\tilde{m} = m + l = \sum_{i=1}^M m_i \quad (10)$$

In light of Equations 9, 10, and 8, the enumeration problem of the nonstandard CNBs (n, m, l) can be essentially converted into the problem of partitioning the three integers \tilde{n} ,

\tilde{m} , and l , along with the subsequent combinatorial arrangements of the obtained parts. In addition, the arrangements of vectors \vec{a} , \vec{b} , and \vec{b}' are subject to the condition that \vec{b} and \vec{b}' should never be adjacent to each other. Otherwise, the resultant path leads to triply fused benzene rings forming a peri-condensed nanobelt instead of the cata-condensed one that we are interested in in the present study. In other words, vectors \vec{b} and \vec{b}' must be always separated by vectors \vec{a} along the construction path. Therefore, we can build the nonstandard CNBs (n, m, l) by taking the standard CNBs (\tilde{n}, \tilde{m}) and replacing L segments of \vec{b} vectors with the same number of \vec{b}' segments. As a result, the following relation holds

$$N = M + L \quad (11)$$

On the basis of the above discussion, the enumeration of the nonstandard CNBs (n, m, l) can be realized using the following procedures. We first enumerate separately all partitions of \tilde{m} and of l and combine each of the partitions of both numbers to form a collected set. As a trick, in the set we have taken the opposite (negative) values of l 's parts in order to distinguish them from \tilde{m} 's parts. We subsequently make all permutations for each array in the collected set. On the other hand, we take all circularly nonequivalent compositions of \tilde{n} , irrespective of clockwise or counterclockwise orderings of \tilde{n} 's parts. Then, we make all valid combinations of the above-obtained compositions of \tilde{n} , \tilde{m} , and l that meet the following two conditions: (i) The N parts of \tilde{n} appear at the odd positions in the sequence of each combination, whereas the numbers coming from the M parts of \tilde{m} and the L parts of l are placed at the even positions; (ii) $N = M + L$ (i.e., Equation 11). Taking each of the valid combinations of \tilde{n} , \tilde{m} and l as a unique path code, we can therefore construct each of the possible isomers of nonstandard CNBs (n, m, l) . In order to distinguish the path code numbers coming from \tilde{n} , \tilde{m} and l , we set a couple of rules for a valid path code of any nonstandard CNB (n, m, l) : (i) The path code numbers at the odd positions come exclusively from the parts of \tilde{n} (corresponding to the steps of \vec{a} in the path), whereas the numbers at the

even positions come either from \tilde{m} 's parts or from l 's parts (corresponding to the \vec{b} steps and \vec{b}' steps, respectively); (ii) If the numbers come from the parts of l , the opposite (negative) numbers are used as the code numbers so as to differentiate them from the parts of \tilde{m} . As the path codes are circularly equivalent (provided that rule (i) is fulfilled), we use the canonical path codes to determine the unique isomers of nonstandard CNBs, similar to the case of standard CNBs. Figure 3 presents the four isomers of CNBs (5, 2, 2) with the corresponding canonical path codes embraced by brackets.

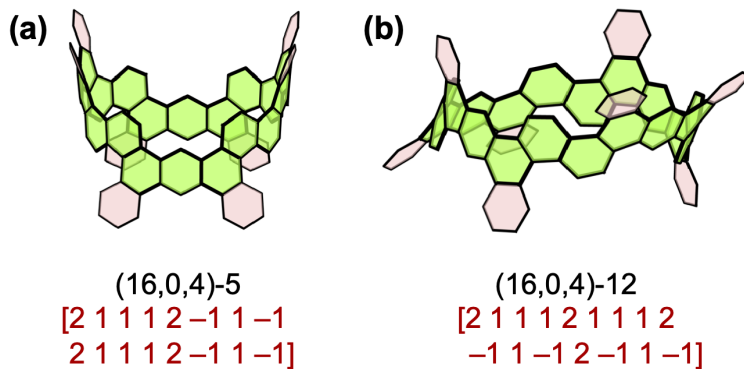


Figure 4. Synthesized nonstandard CNBs (a) $(16,0,4)-5$ and (b) $(16,0,4)-12^{12}$ with their canonical path codes given in square brackets. The essential belt rings are colored in green and the side rings are in pink. Hydrogens and/or substituent groups are not shown.

The nomenclature for the nonstandard CNBs is in analogy to that for the standard CNBs. By sorting the canonical path codes of all isomers of CNBs (n, m, l) , the isomers can be uniquely numbered according their appearance in the sorted list (in lexicographically ascending order). One can check the nomenclature for the four isomers of CNBs (5, 5, 2) in Figure 3. Incidentally, as a consequence of Equations 8–11, the indices (n, m, l) should fulfill at once the following requirements: $n \geq m \geq 0$, $n \geq l + 2$, and $l \geq 1$. All valid indices (n, m, l) for the nonstandard CNBs with up to 10 rings, as well as the corresponding numbers of isomers, are tabulated in Table 2. Furthermore, compared to the standard CNBs, the nonstandard CNBs containing the same number of rings have generally much more isomers. For instance, there are about 25 thousand standard [21]CNBs while this number increases to over 1 million for nonstandard [21]CNBs, as shown in Table 3. We can also see that as the

Table 2. Number of isomers (N_{iso}) of nonstandard CNBs (n, m, l) with the number of rings (NR) ranging from 4 to 10.

NR	(n, m, l)	N_{iso}	NR	(n, m, l)	N_{iso}
4	(3, 0, 1)	1	9	(4, 3, 2)	1
5	(3, 1, 1)	1		(4, 4, 1)	3
	(4, 0, 1)	1		(5, 1, 3)	1
6	(3, 2, 1)	1		(5, 2, 2)	4
	(4, 0, 2)	1		(5, 3, 1)	9
	(4, 1, 1)	2		(6, 0, 3)	2
	(5, 0, 1)	2		(6, 1, 2)	10
7	(3, 3, 1)	1		(6, 2, 1)	10
	(4, 1, 2)	1		(7, 0, 2)	9
	(4, 2, 1)	2		(7, 1, 1)	9
	(5, 0, 2)	2		(8, 0, 1)	3
	(5, 1, 1)	4	10	(4, 4, 2)	1
	(6, 0, 1)	2		(5, 2, 3)	1
8	(4, 2, 2)	1		(5, 3, 2)	4
	(4, 3, 1)	3		(5, 4, 1)	12
	(5, 0, 3)	1		(6, 0, 4)	1
	(5, 1, 2)	3		(6, 1, 3)	4
	(5, 2, 1)	6		(6, 2, 2)	15
	(6, 0, 2)	6		(6, 3, 1)	19
	(6, 1, 1)	6		(7, 0, 3)	9
	(7, 0, 1)	3		(7, 1, 2)	22
				(7, 2, 1)	19
				(8, 0, 2)	17
				(8, 1, 1)	12
				(9, 0, 1)	4

CNB size increases, the number of isomers for the nonstandard CNBs grows more rapidly than that for the standard CNBs. Applying the nomenclature for nonstandard CNBs, the two recently synthesized CNBs¹² can be recognized as (16,0,4)-5 and (b) (16,0,4)-12, as shown in Figure 4a and b.

Table 3. Number of chirality types (N_{chiral}) and total number of isomers (N_{iso}) for the standard and nonstandard CNBs with different numbers of rings (NR) ranging from 3 to 24.

NR	Standard CNBs		Nonstandard CNBs	
	N_{chiral}	N_{iso}	N_{chiral}	N_{iso}
3	2	2	0	0
4	3	4	1	1
5	3	4	2	2
6	4	8	4	6
7	4	9	6	12
8	5	18	8	29
9	5	23	11	61
10	6	44	14	140
11	6	63	17	308
12	7	122	21	697
13	7	190	25	1 572
14	8	362	29	3 570
15	8	612	34	8 180
16	9	1 162	39	18 669
17	9	2 056	44	43 114
18	10	3 914	50	98 974
19	10	7 155	56	229 502
20	11	13 648	62	529 223
21	11	25 482	69	1 230 245
22	12	48 734	76	2 847 701
23	12	92 205	83	6 631 367
24	13	176 906	91	15 397 616

3 Results and Discussion

3.1 Relative Isomer Energies of Standard CNBs

At the GFN2-xTB level of theory (hereafter simply referred to as xTB), we have computed the relative energies for all possible isomers of the standard CNBs containing 3 to 24 rings (see Table 3 for the numbers of isomers). For larger standard CNBs with up to 30 rings, we have prescreened the candidate isomers using a simple and well-performed prediction model that accounts for both the electronic and strain effects on the relative stability of standard CNB isomers (see below for details). As a result, we have considered all isomers with the model predicted relative energy value being less than $0.5|\beta|$, where β is the resonance integral in the Hückel molecular orbital (HMO) theory.^{44–47}

To unveil the factors governing the relative stability of standard CNB isomers, we first examine the xTB computed relative energies, RE_{xTB} , as a function of the total Hückel π energy, E_{HMO} , for all isomers of the same chirality (n, m). Figure 5a plots RE_{xTB} against E_{HMO} for all 257 isomers of CNBs (8,8). We see clearly that the data points are clustered into parallel groups and the points within each group present a good linear correlation between RE_{xTB} and E_{HMO} . It appears that these groups are separated by a constant shift, implying an additional effect on the relative isomer stability apart from the electronic effect approximated by the HMO model. A careful inspection of the structural characteristics reveals that the difference between the groups is linked to the number of turning points (denoted by τ) in the construction path of the corresponding CNB. For example, the lowest-energy isomer, (8,8)-1, with a path code of 16 ones, has 16 turning points in the construction path; every ring in (8,8)-1 serves as a turning point, as can be seen in its 3D structure illustrated in Figure 5c. In comparison, the highest-energy isomer, (8,8)-257, with a path code of [8 8], has only two turning points ($\tau = 2$), as shown in Figure 5d. Comparing the two isomer structures shown embedded in a (8,8) CNT in Figure 5c,d, we notice that (8,8)-257 is a structurally high aspect ratio CNB³¹ and has thus a much larger circumference than (8,8)-1. We would

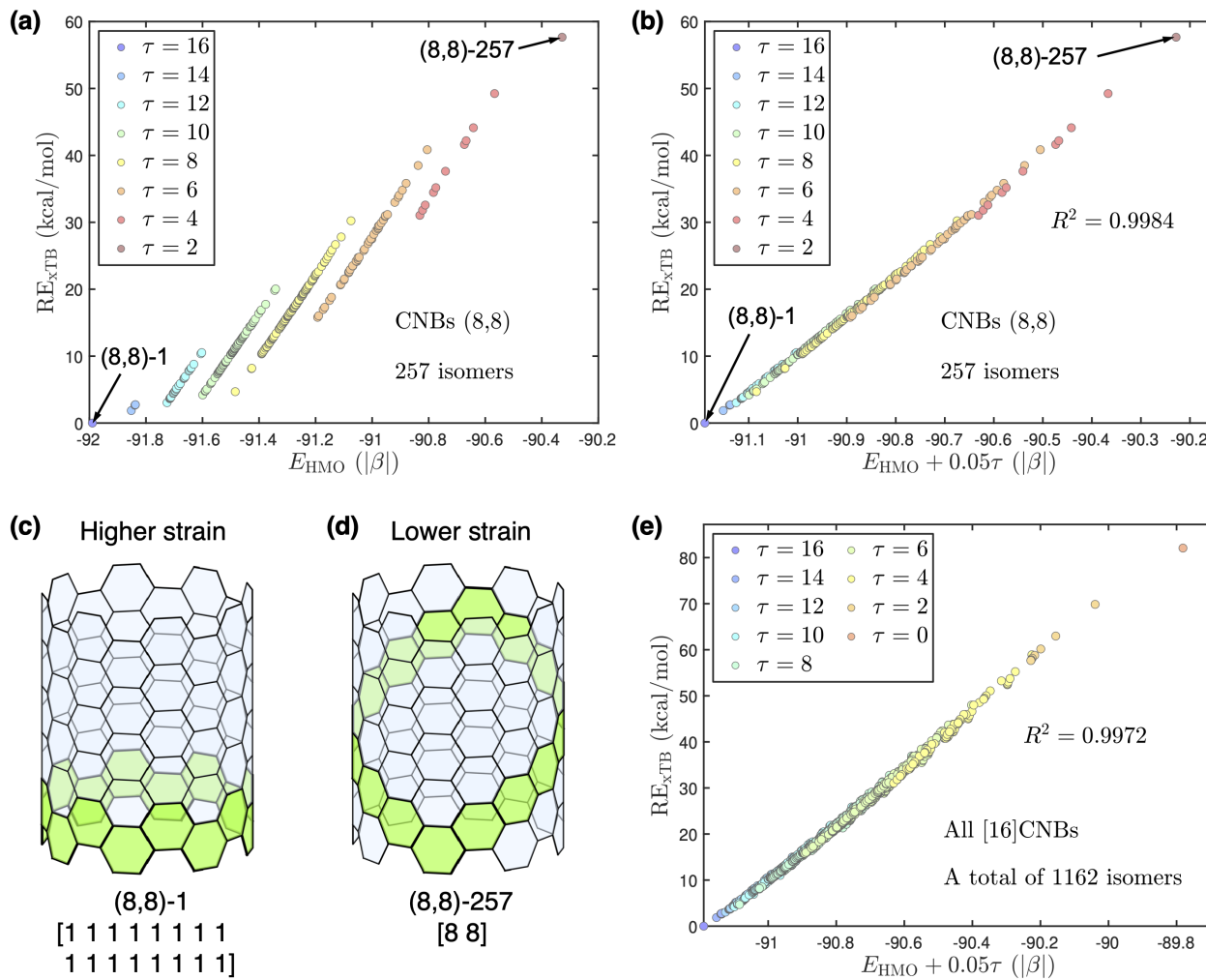


Figure 5. (a) XTB computed relative energy, RE_{XTB}, versus HMO π energy, E_{HMO} , for all 257 isomers of CNBs (8,8). The data points are distinguished by different colors, according to the number of turning points (τ) in the construction path. (b) RE_{XTB} plotted against $E_{HMO} + 0.05|\beta|\tau$ for all CNB (8,8) isomers (see Equation 12). (c) and (d) Structures of CNB isomers (8,8)-1 and (8,8)-257, respectively, depicted within a segment of nanotube (8,8). The path codes are given in squared bracketed. (e) Correlation between RE_{XTB} and $(E_{HMO} + 0.05|\beta|\tau)$ for all 1162 isomers of [16]CNBs with all kinds of chiralities. Squared correlation coefficients, R^2 , are provided in (b) and (e).

thus expect that the latter isomer (with $\tau = 16$) suffers from a greater strain effect than the former ($\tau = 2$). More generally, CNB isomers with more turning points (i.e., a larger τ value) should be more destabilized by the strain in macrocyclic skeleton, which well explains the systematic shift between the groups shown in Figure 5a.

To quantitatively confirm the above speculation, we propose a simple model to predict

the relative stability of standard CNB isomers, combining both the π electronic effect (as described by the HMO theory) and the strain effect (assumed to be proportional to τ), as follows

$$E_{\text{model}}^{\text{std}} = E_{\text{HMO}} + 0.05\tau \quad (12)$$

where both E_{HMO} and the empirical coefficient 0.05 are in units of $|\beta|$. The last term in the equation, 0.05τ , is responsible for the shift between groups seen in Figure 5a. Adding this strain effect term to E_{HMO} results in a very good correlation with the xTB relative energy (the squared correlation coefficient R^2 being 0.9984), as evidenced in Figure 5b. Even for all 1162 isomers of [16]CNBs including all possible chirality types, the strain-corrected E_{HMO} correlates equally well with RE_{xTB} ($R^2 = 0.9972$), as we can see in Figure 5e. In fact, employing the universal empirical parameter 0.05, the simple model exhibits high prediction performance for all considered standard CNB isomers containing 5 or more rings. The squared correlation coefficients are above 0.9 in all cases and are as high as 0.99 for CNBs with more than 8 rings (see [Figures S1–S5 in Supporting Information](#)).

Therefore, we conclude that the relative stability of standard CNB isomers is essentially governed by two opposite effects, the π electronic stabilization offered by the conjugated system in the entire molecule and the strain destabilization induced by the curved macrocyclic shape. We also infer that the electronic effect prevails over the strain effect and the reason is as follows. As we can see from the groups associated with different τ values in Figure 5a, the CNB isomers with more turning points have generally more favorable π electronic effect (i.e., lower value of E_{HMO}) but meanwhile unfavorable strain effect (due to a shorter circumference of the macrocycle). Overall, as revealed in Figure 5b and e, the isomers with more turning points are in general lower in energy than those with fewer turning points, indicating the more decisive role of the π electronic effect than the strain effect.

The fact that the CNB isomers with fewer turning points benefit less from π stabilization

can be understood by the Fries rule^{48–52} or the Clar rule.^{53–55} According to the Clar rule, given a π conjugated polycyclic system, one tries to allocate as many Clar sextets to the rings as possible, while utilizing the remaining π electrons to form a valid, closed-shell Kekulé structure. Each Clar sextet comprises formally six π electrons within a ring and is symbolized by a circle inscribing the ring. Note that no two Clar sextets are adjacent; otherwise, one double counts the π electrons from the adjacent C atoms between two neighboring rings. Such a resonance structure with the maximum possible number of Clar sextets is called a Clar structure. The Clar rule posits that the more sextets a π conjugated molecule possesses in its Clar structures, the more π electronic stabilization it acquires. For the looped macrocycles like CNBs with NR rings, the maximum possible number of Clar sextets is $NR/2$ since the Clar sextets and nonsextets are distributed alternately in the rings. It is easy to show that in a segment comprised of three or more linearly arranged rings (taking anthracene as the simplest example), one can draw only one Clar sextet without introducing radical sites (with unpair electrons) to the Clar structure.⁵⁴ Hence, if a segment of a conjugated benzenoid contains more than three rings in a row (like naphthacene), there are more nonsextet rings than sextet rings and hence the molecule is deficient in π electronic stabilization. As the length of the segment of linearly arranged rings increases, the percentage of sextet rings reduces, thus producing weaker π stabilization effect. As for CNBs, each path segment in the construction path consists of a certain number of linearly arranged rings. Accordingly, for the CNB isomers with a given number of rings, those having fewer turning points in the construction path have fewer but longer path segments and are therefore electronically less stable.

3.2 HOMO–LUMO Gaps of Standard CNBs

While the thermodynamic stability can be measured by the relative energy, we would also like to examine the kinetic reactivity of CNBs on the basis of their HOMO–LUMO gaps, which are also referred to as chemical hardness^{56–58} in conceptual DFT^{59–61} and may usually

reflect chemical reactivity.^{62,63}

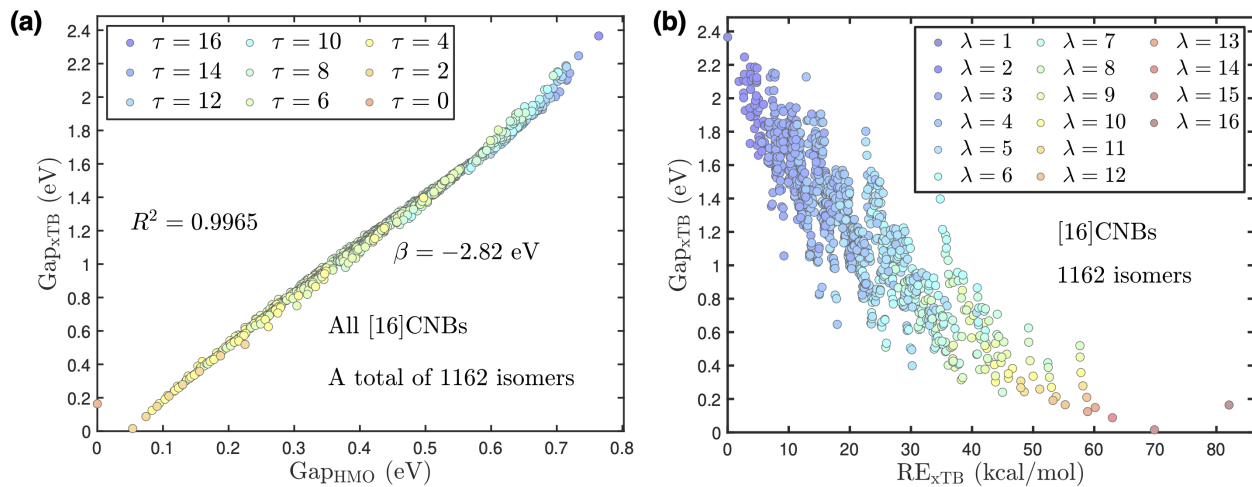


Figure 6. (a) XTB computed HOMO–LUMO gap, Gap_{xTB} , versus HMO HOMO–LUMO gap, Gap_{HMO} , for all 1162 isomers of [16]CNBs with all chirality types. Isomers with different numbers of turning points (τ) in the construction path are indicated by different colors. (b) Gap_{xTB} versus xTB relative energy, RE_{xTB} , for all isomers of [16]CNBs. The data points are colored according to the maximum number in the path code, λ .

We present in Figure 6a HOMO–LUMO gaps for all isomers of the standard [16]CNBs obtained from the xTB and HMO calculations. As we can see, the HMO gaps (in units of $|\beta|$) correlates very well with the xTB calculated gaps ($R^2 = 0.9965$). A least-squares fit to the correlation gives an estimation of β , being -2.82 eV for [16]CNBs. We have similarly estimated the values of β for CNBs of other sizes (see [Table S2 in Supporting Information](#)), which fall into a reasonable range for typical π conjugated carbon systems.^{64,65} Figure 6b plots the xTB computed HOMO–LUMO gaps versus the xTB relative energies for [16]CNB isomers. The overall tendency suggests that the thermodynamic stability generally coincides with the kinetic stability for CNBs; lower-energy isomers are more likely to exhibit a higher HOMO–LUMO gap, and vice versa. This conclusion holds for the standard CNBs of other sizes (see [Figures S9–S12 in Supporting Information](#)).

Furthermore, Figure 6a discloses that, in general, the isomers with more turning points (a larger τ value) possess a larger HOMO–LUMO gap. In Figure 6b, we have colored the data points according to the maximum number in the path code (λ). It is evident that the

isomers with a smaller λ generally have a lower relative energy and a larger HOMO–LUMO gap, which can be understood using the Clar rule. A smaller maximum number in the path code, λ , implies that the CNB isomer has more short segments that consist of fewer linearly arranged rings and therefore a higher sextets to nonsextets ratio. As a result of the Clar rule, the isomers with a smaller value of λ (and as a consequence, usually with a larger value of τ) are electronically more favored, showing a higher stability and opening a larger gap. The ideal case is the first isomer of armchair CNBs, (n,n) -1, whose path code is $2n$ ones (see Figure 5c for the example of CNB (8,8)-1). It has the shortest path segments (all being 1 and hence $\lambda = 1$) and a maximum possible number of turning points ($\tau = 2n$). Thus, the armchair CNB isomer (n,n) -1 has a maximized π stabilization effect and are the lowest-energy form of all considered CNBs with an even number of rings ($NR = 2n$). As for CNBs containing an odd number of rings, the lowest-energy structure is found to be isomer $(n+1,n)$ -1, since its has the longest path code ($\tau = 2n$) composed of a 2 followed by $(2n-1)$ ones.

On the contrary, the isomers with longer path segments (i.e., with a larger λ) are less stabilized electronically due to the fewer Clar sextets they acquire. If a segment of a CNB comprises over six rings in a row, the HOMO–LUMO gap is expected to be so narrow that the electronic ground state is most likely an open-shell singlet with a polyyradical character. Similar phenomenon has been found in the case of linear oligoacenes,⁶⁶ generalized infinitenes,²⁰ and generalized kekulenes.²¹ The extreme case is the zigzag CNBs $(n,0)$, or the so-called $[n]$ cyclacenes.²⁶ The absence⁶⁷ of Clar sextets in their electronic structure makes them the highest-energy isomers for all sizes of CNBs. Our DFT calculations reveal that the zigzag CNBs with 5 or more rings have an open-shell singlet ground state, in line with the previous studies.^{68–70} As previous multiconfigurational computations⁶⁹ disclosed, zigzag CNBs have an increasing polyyradical character with the increasing number of rings.

Interestingly, the three experimentally synthesized armchair CNBs, $(6,6)$ -16,^{28,30} $(8,8)$ -108,³⁰ and $(12,12)$ -12235,³⁰ (see Figure 2a, b, and d, respectively), all achieve the maximum

number ($NR/2$) of Clar sextets, or say, 50% of the rings are aromatic sextets. As for the other CNBs synthesized so far^{13,18,19,31} (Figure 2c, e, and h), the essential belt structure owns an insufficient number of Clar sextets and is supposed to be unstable. This explains why side rings are attached to the essential belt in the synthesized structures, which increases the percentage of sextet rings and thereby enhances the stability. For instance, owing to the additional side rings, the synthesized CNBs, (8,8)-201,³¹ (12,12)-28670,¹⁸ and (18,12)-1,¹⁸ have increased the sextet percentage from 37.5%, 25.0%, and 40.0%, respectively, to 54.5%, 57.1%, and 57.1%, respectively. Remarkably, in the synthesized zigzag CNBs, (12,0)-1¹³ and (18,0)-1¹⁹ (Figure 2f,g), the attachment of side rings to the otherwise sextet-free zigzag belts brings about a considerable number of Clar sextets occupying 60% of the rings.

3.3 Relative Stabilities of Nonstandard CNBs

To systematically explore the relative stabilities of nonstandard CNBs, we have performed xTB calculations on all possible isomers of all sizes up to $NR = 12$. For larger nonstandard CNBs with 13 to 21 rings, we have only considered the isomers with a path code consisting of numbers no greater than 2 (i.e., $\lambda \leq 2$). This selection criterion ensures that all candidate isomers achieve a maximum possible number (equal to $NR/2$) of Clar sextets in order to have optimal electronic stability. When the CNB size further grows, the number of possible isomers is enormous, e.g., over 15 million for the nonstandard [24]CNBs (see Table 3). Therefore, for the nonstandard CNBs with 22 to 29 rings, we have chosen only the structures that have $\lambda \leq 2$ and do not contain any benzo[c]phenanthrene-like motif to avoid strong H···H repulsion (see Figure 7c and the discussion below for detailed reasons).

We first look at the correlation between the xTB relative isomer energies and the HMO energies, as shown in Figure 7a for all 90 isomers of CNB (8, 2, 2). Although the data points are distributed into groups associated with the number of turning points, τ , no universal correlation is seen between RE_{xTB} and E_{HMO} for all different groups, which is unlike the case of standard CNBs (see Figure 5a). For example, the data points belonging to the

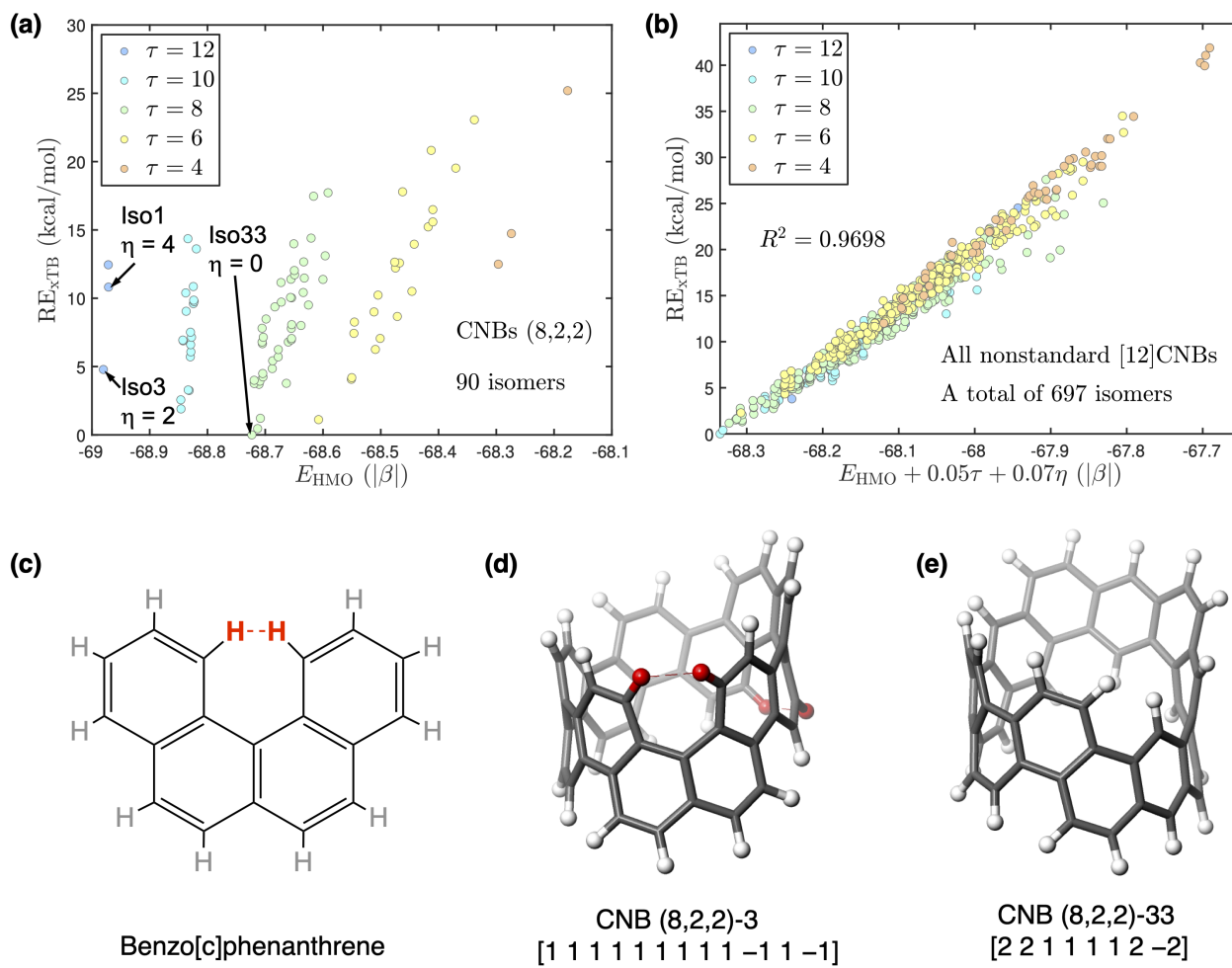


Figure 7. (a) XTB relative energy, RE_{xTB} , versus HMO π energy, E_{HMO} , for all 90 isomers of the nonstandard CNBs (8,2,2). The data points are colored according to the number of turning points (τ) in the CNB structures. (b) Correlation between RE_{xTB} and $E_{HMO} + 0.05|\beta|\tau + 0.07|\beta|\eta$ (i.e., Equation 13) for all 697 isomers of nonstandard [12]CNBs with all kinds of chiralities. Squared correlation coefficient, R^2 , is indicated. (c) Structural formula of the benzo[c]phenanthrene molecule, where the closest $H \cdots H$ contact is indicated in red. (d) and (e) Structures of CNB isomers (8,2,2)-3 and (8,2,2)-33, respectively. The canonical path codes are given in squared brackets. In (d), isomer (8,2,2)-3 has two pairs of close $H \cdots H$ contact, as highlighted in red.

$\tau = 10$ group are distributed almost vertically (see the cyan points in Figure 7a), indicating that these isomers have very similar E_{HMO} values and the same τ value, but their relative energies, RE_{xTB} , span a considerable range of ca. 12 kcal/mol. This hints that, aside from the electronic stabilization and strain destabilization effects, there exists a third factor affecting noticeably the relative stability of nonstandard CNB isomers.

After scrutinizing the structural characteristics of CNB (8, 2, 2) isomers, we found that the relative energy depends also on the number of close H···H contacts, like the one present in the benzo[c]phenanthrene molecule. It has been known that the overcrowding in the fjord-regions of benzo[c]phenanthrene causes considerable H···H repulsion,⁷¹ as shown in Figure 7c. As a consequence, this molecule adopts a distorted geometry rather than a planar one in order to alleviate the H···H repulsion. The dihedral angle between its two terminal rings is about 28.1° according to our DFT calculation, in good accordance with the experimental value (26.7°) in crystal state measured by X-ray crystallographic analysis.⁷² By contrast, the isomeric chrysene molecule is perfectly planar and our DFT calculation shows that it is 5.3 kcal/mol lower in energy than benzo[c]phenanthrene. Similar phenomenon is found in certain nonstandard CNBs. Taking CNB isomer (8, 2, 2)-3 as an example, it has two pairs of benzo[c]phenanthrene-like close H···H contacts, as indicated in red in Figure 7d. In comparison, isomer (8, 2, 2)-1 contains four benzo[c]phenanthrene motifs and is therefore expected to suffer from higher distortion strain induced by H···H repulsion. Hence, it is now understandable that isomer (8, 2, 2)-1 is markedly less stable than isomer (8, 2, 2)-3 (see Figure 7a), albeit both have very similar HMO energies and the same number of turning points ($\tau = 12$). Regarding the lowest-energy isomer, (8, 2, 2)-33 (Figure 7e), despite its relatively higher HMO energy, the absence of close H···H contacts makes it energetically more stable than (8, 2, 2)-1, as can be seen in Figure 7a.

Incorporating the destabilization effect caused by H···H repulsion, we come up with the following model for predicting the relative isomer stability of nonstandard CNBs by adding an additional term to Equation 12:

$$E_{\text{model}}^{\text{nonstd}} = E_{\text{HMO}} + 0.05\tau + 0.07\eta \quad (13)$$

where η is the number of benzo[c]phenanthrene motifs in the carbon framework and the corresponding coefficient takes an empirical value of 0.07 (in units of $|\beta|$). This model

works generally well for nonstandard CNBs of many other sizes, as shown in [Figures S6–S8 in Supporting Information](#). From Equation 13, we can see that the term accounting for close H···H contacts, 0.07η , is roughly of equal importance to the strain-related term, 0.05τ . Thus, a stable nonstandard CNB should ideally contain no benzo[c]phenanthrene motif ($\eta = 0$), which is corroborated by the fact that the benzo[c]phenanthrene motif is absent in the nonstandard CNBs synthesized so far¹² (see Figure 4).

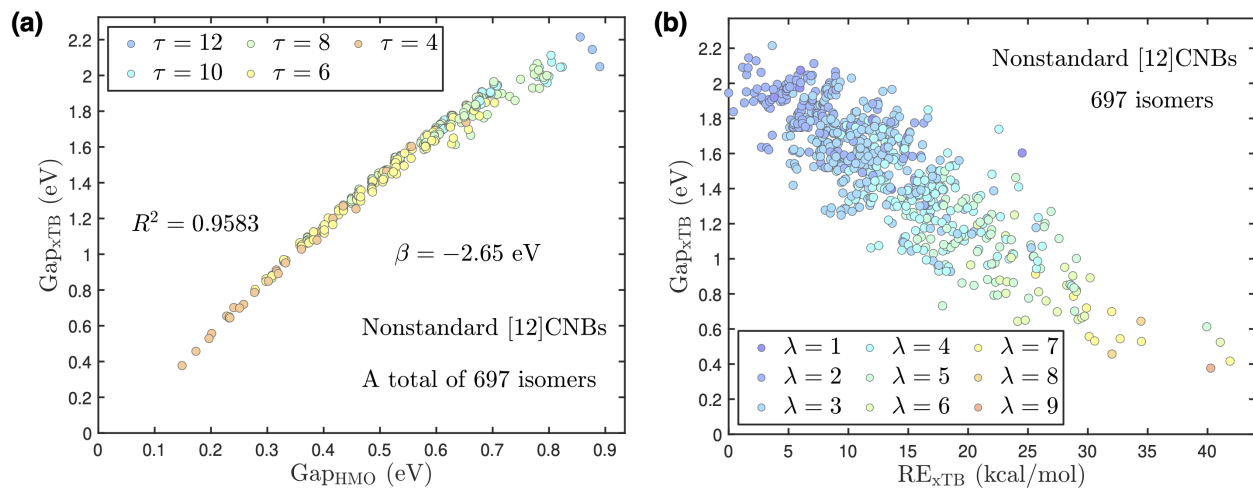


Figure 8. (a) XTB HOMO–LUMO gap, Gap_{xTB} , versus HMO HOMO–LUMO gap, Gap_{HMO} , for all 697 isomers of nonstandard [12]CNBs with all kinds of chiralities. Isomers with different numbers of turning points (τ) in the construction path are colored differently. (b) Gap_{xTB} versus xTB relative energy, RE_{xTB} , for all isomers of nonstandard [12]CNBs. The data points are colored according to the maximum number in the path code, λ .

We have also investigated the HOMO–LUMO gaps of the nonstandard CNBs and the basic conclusions are similar to those for the standard CNBs. Figure 8a attests a good correlation between the xTB and the HMO gaps for all 697 isomers of the nonstandard [12]CNBs. In Figure 8b, we find a general tendency similar to that in the case of standard CNBs (cf. Figure 6b); the lower-energy isomers usually exhibit a larger HOMO–LUMO gap and the isomers with smaller λ are more stable both thermodynamically and kinetically. The latter fact can likewise be explained by the Clar sextet rule. The same conclusions hold as well for the nonstandard CNBs of other sizes, as evident in [Figure S13 in Supporting Information](#).

3.4 Relative energy distribution and lowest-energy forms of CNBs

Considering that there are typically a huge number of isomers for both the standard and nonstandard CNBs, we are curious about how their relative energies are distributed. Figure 9a presents the probability density distribution of the xTB relative energies of all 176 906 isomers of the standard CNBs of all chiralities. The histogram exhibits a slightly right-skewed distribution, which can be best described by a reversed Weibull distribution (see the blue solid curve in Figure 9a). This indicates that most of the isomers have intermediate relative energies and there are more isomers with a relative energy lower than the mean value. Similar distribution is observed for the relative energies of nonstandard CNB isomers, as shown in Figure 9b for the nonstandard [12]CNBs. The asymmetric relative energy distribution for CNB isomers might be explained as follows. As discussed in the preceding subsections, isomers with shorter path segments in the construction path (i.e., with a smaller λ) are generally lower in energy. Meanwhile, shorter path segments usually indicate that there are more segments/turning points (i.e., a larger τ) and hence a larger number of combinations of them to constitute the whole path, thus resulting in a larger number of possible isomers. Therefore, lower-energy isomers tend to be more abundant than the higher-energy ones. Taking into account this tendency on top of the normal distribution (black dashed curves in Figure 9) would lead to the right-skewed distribution. It is interesting to mention that the relative energies of fullerene isomers (like C₆₀ and C₈₀) also follow an analogous right-skewed distribution.⁷³

Lastly, we pay attention to the lowest-energy isomers of CNBs. As mentioned above, the lowest-energy form of the standard CNBs shows a quite regular pattern: they correspond to the isomer (n, n)-1 and isomer (n + 1, n)-1, respectively, for the CNBs with an even number of rings and those with an odd number of rings (see Table 4). However, there is no discernible regularity for the lowest-energy isomer of the nonstandard CNBs, probably due to the large number of nearly isoenergy isomers and the subtle interplay among the different stability factors. As we can see in Table 4, the lowest-energy form of nonstandard CNBs can

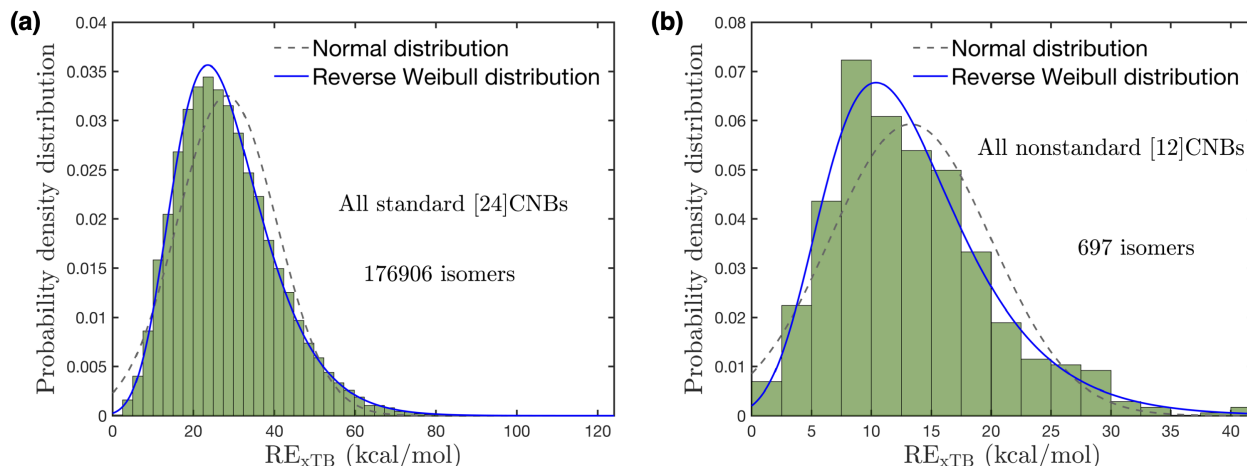


Figure 9. Probability density distribution of the xTB relative energies of all isomers of (a) standard [24]CNBs and (b) nonstandard [12]CNBs. The bins of the histograms are 2.5 kcal/mol. The black dashed and the blue solid curves correspond, respectively, to the normal distribution and the reverse Weibull distribution fitted to the actual distribution.

have different chiralities varying with the CNB size; in most cases it is of chiral type and occasionally it is of zigzag type. Comparing both the standard and nonstandard CNBs, we see in Table 4 a general trend that for smaller sizes the lowest-energy nonstandard isomer is a considerably higher in energy than the lowest-energy standard isomer. As the CNB size increases, the energy difference between the lowest-energy nonstandard and standard isomers decreases and becomes less than ca. 2 kcal/mol for $NR \geq 13$. For sufficiently large ($NR \geq 17$) CNBs with an odd number of rings, the lowest-energy nonstandard isomer is even slightly lower in energy than the standard one. At any rate, the energy difference is practically insignificant between the lowest-energy isomers of nonstandard and standard CNBs. Hence, from a thermodynamic point of view, both the standard and nonstandard forms of relatively large CNBs are suggested to be viable synthetic targets.

Table 4. Chirality and relative energy (in kcal/mol) of the lowest-energy isomer for the standard and nonstandard CNBs with a varying number of rings (NR). Relative energies in brackets are obtained from DFT calculations including zero-point energy correction.

NR	Std. CNBs	Nonstd. CNBs	NR	Std. CNBs	Nonstd. CNBs
4	(2, 2) [0.0]	(3, 0, 1) [46.9]	16	(8, 8) [0.0]	(12, 1, 3) [1.6]
5	(3, 2) [0.0]	(3, 1, 1) [36.8]	17	(9, 8) [0.1]	(11, 4, 2) [0.0]
6	(3, 3) [0.0]	(5, 0, 1) [15.6]	18	(9, 9) [0.0]	(14, 0, 4) [1.2]
7	(4, 3) [0.0]	(4, 2, 1) [15.3]	19	(10, 9) [0.3]	(14, 1, 4) [0.0]
8	(4, 4) [0.0]	(6, 1, 1) [7.8]	20	(10, 10) [0.0]	(15, 1, 4) [1.0]
9	(5, 4) [0.0]	(6, 2, 1) [6.9]	21	(11, 10) [0.4]	(15, 2, 4) [0.0]
10	(5, 5) [0.0]	(7, 2, 1) [4.6]	22	(11, 11) [0.0]	(17, 0, 5) [0.9]
11	(6, 5) [0.0]	(8, 1, 2) [3.2]	23	(12, 11) [0.5]	(16, 3, 4) [0.0]
12	(6, 6) [0.0]	(8, 3, 1) [3.3]	24	(12, 12) [0.0]	(18, 1, 5) [0.9]
13	(7, 6) [0.0]	(9, 2, 2) [1.1]	25	(13, 12) [0.4]	(17, 4, 4) [0.0]
14	(7, 7) [0.0]	(11, 0, 3) [2.2]	26	(13, 13) [0.0]	(20, 0, 6) [0.9]
15	(8, 7) [0.0]	(10, 3, 2) [0.2]	27	(14, 13) [0.3]	(18, 5, 4) [0.0]

4 Conclusions

In summary, we have devised a graph-based method to enumerate all possible isomers of standard CNBs with any given chirality (n, m). This approach elegantly converts the structural construction of CNBs into a problem of integer partitions coupled with combinatorics of numbers. By introducing an additional winding index, l , we can extend the standard CNBs to the nonstandard CNBs, delineated by the triplet indices, (n, m, l) . Allowing $l = 0$, we can incorporate the standard CNBs (n, m) into the general notation, $(n, m, 0)$. Each of the standard and nonstandard CNBs can be uniquely described by a canonical path code that instructs us how to cut out the CNB segment from the corresponding CNT sidewall. Based on the lexicographic ordering of the canonical path codes, we have proposed a systematic nomenclature for CNBs and demonstrated its efficacy in naming the synthesized CNB structures known to date. This naming system should be also applicable to the partially saturated CNBs, heteroatom-embedded CNBs, or other related CNB structures.

On the basis of exhaustive xTB calculations of the standard CNB isomers containing up to 30 rings, we have established a simple, efficient, and well performed model to quantitatively predict the relative isomer stability, requiring only the topological information (the path code) of CNBs. More profoundly, the model clearly discloses that the relative stability of standard CNBs is essentially governed by the π conjugation stabilization and the strain destabilization due to the rigid carbon framework. In some nonstandard CNBs emerges a third destabilizing factor, the H \cdots H repulsion in the benzo[c]phenanthrene-like regions. By including this effect, we have formulated an extended model that also shows a high predictive power for the relative stability of the nonstandard CNBs. Remarkably, all three stability effects can be approximately linked to topological characteristics: the π stabilization can be understood by the Clar rule; the strain effect is roughly proportional to the number of turning points in CNB's construction path; the H \cdots H repulsion can be estimated by counting the close H \cdots H contacts. As a result, we put forward two simple criteria as prerequisite for a stable CNB structure: i) all path segments should not be longer than 2 ($\lambda \leq 2$); ii) no

benzo[c]phenanthrene-like motif is present ($\eta = 0$).

To evaluate the relative kinetic stability of CNB isomers, we have examined systematically their HOMO–LUMO gaps, which show a general correlation with the relative energies. Hence, we conclude that the thermodynamic stability of CNBs generally coincides with their kinetic stability.

Finally, we have discovered that the relative energies of CNB isomers follows a slightly right-skewed distribution. For all considered standard CNBs, the lowest-energy isomer is always (n, n) -1 (for even number of rings) or $(n + 1, n)$ -1 (for odd number of rings). As for the nonstandard CNBs, however, no clear pattern is observed for the lowest-energy isomeric forms. In conclusion, we suggest that both the standard and nonstandard CNBs can be considered as reasonable candidates for future synthesis.

5 Computational Methods

We fully optimized at the GFN2-xTB^{74,75} level the geometries of all considered CNB isomers, followed by vibrational frequency analysis for verification of true energy minima. On the basis of the xTB calculations, we chose the at least 50 lowest energy isomers of each size of the standard CNBs and those of the nonstandard CNBs for further geometry optimization and vibrational frequency analysis at the B3LYP^{76,77}/6-31G(d) level that includes Grimme's DFT-D3 dispersion correction (with Becke–Johnson damping).⁷⁸ We have shown in previous work²⁰ that the DFT method adopted here produces the relative energies for various types of looped cycloarenes that are in good agreement with the higher level ω B97XD/cc-pVDZ results. The GFN2-xTB method has also been shown to be reliable for predicting the relative isomer stability for generalized infinitenes,²⁰ generalized kekulenes,²¹ and clarenes,²¹ as well as different types of CNBs considered in this study (see [Figures S14 and S15 in Supporting Information](#)).

6 Data and Software Availability

We carried out all xTB and DFT calculations using the XTB 6.3.3⁷⁹ and the GAUSSIAN 16⁸⁰ programs, respectively. We employed our open-source software EZRESON (version 3.0)^{52,55,81–83} to enumerate the Clar structures and determine the number of Clar sextets. Most of the data analysis was performed and the resultant graphs were created with the aid of the MATLAB software.⁸⁴ The 3D molecular structures were rendered and drawn using the open-source Jmol software.⁸⁵

Supporting Information Available

Number of isomers and chirality types for standard CNBs; model predicted relative energies for CNB isomers; comparison between xTB and HMO HOMO–LUMO gaps; xTB HOMO–LUMO gaps versus xTB relative energies; comparison between DFT and xTB relative energies.

Acknowledgement

This work was financially supported by National Natural Science Foundation of China (22073080), and Double Innovation Talent Program of Jiangsu Province (JSSCRC2021542).

References

- (1) Cheung, K. Y.; Segawa, Y.; Itami, K. Synthetic Strategies of Carbon Nanobelts and Related Belt-Shaped Polycyclic Aromatic Hydrocarbons. *Chem. Eur. J.* **2020**, *26*, 14791–14801.
- (2) Guo, Q.-H.; Qiu, Y.; Wang, M.-X.; Fraser Stoddart, J. Aromatic hydrocarbon belts. *Nat. Chem.* **2021**, *13*, 402–419.

- (3) Li, Y.; Kono, H.; Maekawa, T.; Segawa, Y.; Yagi, A.; Itami, K. Chemical Synthesis of Carbon Nanorings and Nanobelts. *Acc. Mater. Res.* **2021**, *2*, 681–691.
- (4) Imoto, D.; Yagi, A.; Itami, K. Carbon Nanobelts: Brief History and Perspective. *Precision Chemistry* **2023**,
- (5) Zhang, R.; An, D.; Zhu, J.; Lu, X.; Liu, Y. Carbon Nanorings and Nanobelts: Material Syntheses, Molecular Architectures, and Applications. *Adv. Funct. Mater.* **2023**, *33*, 2305249.
- (6) Lewis, S. E. Cycloparaphenylenes and related nanohoops. *Chem. Soc. Rev.* **2015**, *44*, 2221–2304.
- (7) Zhang, R.; Zhu, J.; An, D.; Lu, X.; Liu, Y. Synthetic strategies and applications towards carbon nanorings and carbon nanobelts. *Sci. Bull.* **2023**, *68*, 247–250.
- (8) Segawa, Y.; Yagi, A.; Ito, H.; Itami, K. A Theoretical Study on the Strain Energy of Carbon Nanobelts. *Org. Lett.* **2016**, *18*, 1430–1433.
- (9) Shi, T.-H.; Guo, Q.-H.; Tong, S.; Wang, M.-X. Toward the Synthesis of a Highly Strained Hydrocarbon Belt. *J. Am. Chem. Soc.* **2020**, *142*, 4576–4580.
- (10) Nogami, J.; Tanaka, Y.; Sugiyama, H.; Uekusa, H.; Muranaka, A.; Uchiyama, M.; Tanaka, K. Enantioselective Synthesis of Planar Chiral Zigzag-Type Cyclophenylene Belts by Rhodium-Catalyzed Alkyne Cyclotrimerization. *J. Am. Chem. Soc.* **2020**, *142*, 9834–9842.
- (11) Zhang, Q.; Zhang, Y.-E.; Tong, S.; Wang, M.-X. Hydrocarbon Belts with Truncated Cone Structures. *J. Am. Chem. Soc.* **2020**, *142*, 1196–1199.
- (12) Xia, Z.; Pun, S. H.; Chen, H.; Miao, Q. Synthesis of Zigzag Carbon Nanobelts through Scholl Reactions. *Angew. Chem. Int. Ed.* **2021**, *60*, 10311–10318.

- (13) Han, Y.; Dong, S.; Shao, J.; Fan, W.; Chi, C. Synthesis of a Sidewall Fragment of a (12,0) Carbon Nanotube. *Angew. Chem. Int. Ed.* **2021**, *60*, 2658–2662.
- (14) Lin, J.; Wang, S.; Zhang, F.; Yang, B.; Du, P.; Chen, C.; Zang, Y.; Zhu, D. Highly efficient charge transport across carbon nanobelts. *Sci. Adv.* **2022**, *8*, eade4692.
- (15) George, G.; Stasyuk, O. A.; Solà, M.; Stasyuk, A. J. A step towards rational design of carbon nanobelts with tunable electronic properties. *Nanoscale* **2023**, *15*, 17373–17385.
- (16) Vögtle, F. Cyclophanes II. Topics in Current Chemistry. *Top. Curr. Chem.* **1983**, *115*, 157.
- (17) Vögtle, F.; Schröder, A.; Karbach, D. Strategy for the Synthesis of Tube-Shaped Molecules. *Angew. Chem. Int. Ed. in English* **1991**, *30*, 575–577.
- (18) Cheung, K. Y.; Gui, S.; Deng, C.; Liang, H.; Xia, Z.; Liu, Z.; Chi, L.; Miao, Q. Synthesis of Armchair and Chiral Carbon Nanobelts. *Chem* **2019**, *5*, 838–847.
- (19) Cheung, K. Y.; Watanabe, K.; Segawa, Y.; Itami, K. Synthesis of a zigzag carbon nanobelt. *Nat. Chem.* **2021**, *13*, 255–259.
- (20) Du, K.; Wang, Y. Infinitenes as the Most Stable Form of Cycloarenes: The Interplay among π Delocalization, Strain, and $\pi-\pi$ Stacking. *J. Am. Chem. Soc.* **2023**, *145*, 10763–10778.
- (21) Du, K.; Wang, Y. Generalized kekulenes and clarenes as novel families of cyclarenes: structures, stability, and spectroscopic properties. *Phys. Chem. Chem. Phys.* **2023**, *to be submitted*.
- (22) Fan, W.; Han, Y.; Wang, X.; Hou, X.; Wu, J. Expanded Kekulenes. *J. Am. Chem. Soc.* **2021**, *143*, 13908–13916.
- (23) Krzeszewski, M.; Ito, H.; Itami, K. Infinitene: A Helically Twisted Figure-Eight [12]Circulene Topoisomer. *J. Am. Chem. Soc.* **2022**, *144*, 862–871.

- (24) Fan, W.; Matsuno, T.; Han, Y.; Wang, X.; Zhou, Q.; Isobe, H.; Wu, J. Synthesis and Chiral Resolution of Twisted Carbon Nanobelts. *J. Am. Chem. Soc.* **2021**, *143*, 15924–15929.
- (25) Zhou, Q.; Hou, X.; Wang, J.; Ni, Y.; Fan, W.; Li, Z.; Wei, X.; Li, K.; Yuan, W.; Xu, Z.; Zhu, M.; Zhao, Y.; Sun, Z.; Wu, J. A Fused [5]Helicene Dimer with a Figure-Eight Topology: Synthesis, Chiral Resolution, and Electronic Properties. *Angew. Chem. Int. Ed.* **2023**, *62*, e202302266.
- (26) Heilbronner, E. Molecular Orbitals in homologen Reihen mehrkerniger aromatischer Kohlenwasserstoffe: I. Die Eigenwerte von LCAO-MO's in homologen Reihen. *Helv. Chim. Acta* **1954**, *37*, 921–935.
- (27) Iyoda, M.; Kuwatani, Y.; Nishinaga, T.; Takase, M.; Nishiuchi, T. *Fragments of Fullerenes and Carbon Nanotubes*; 2011; pp 311–342.
- (28) Povie, G.; Segawa, Y.; Nishihara, T.; Miyauchi, Y.; Itami, K. Synthesis of a carbon nanobelt. *Science* **2017**, *356*, 172–175.
- (29) (6,6)Carbon Nanobelt Bis(tetrahydrofuran) Adduct. CAS RN: 2245104-25-8; I1078; Tokyo Chemical Industry Co., Ltd.: Tokyo. 2023; <https://www.tcichemicals.com/JP/en/p/I1078>.
- (30) Povie, G.; Segawa, Y.; Nishihara, T.; Miyauchi, Y.; Itami, K. Synthesis and Size-Dependent Properties of [12], [16], and [24]Carbon Nanobelts. *J. Am. Chem. Soc.* **2018**, *140*, 10054–10059.
- (31) Bergman, H. M.; Kiel, G. R.; Handford, R. C.; Liu, Y.; Tilley, T. D. Scalable, Divergent Synthesis of a High Aspect Ratio Carbon Nanobelt. *J. Am. Chem. Soc.* **2021**, *143*, 8619–8624.

- (32) Shudo, H.; Kuwayama, M.; Segawa, Y.; Itami, K. Synthesis of cyclooctylenes from carbon nanobelts. *Chem. Sci.* **2020**, *11*, 6775–6779.
- (33) Yamashina, M.; Tanaka, Y.; Lavendomme, R.; Ronson, T. K.; Pittelkow, M.; Nitschke, J. R. An antiaromatic-walled nanospace. *Nature* **2019**, *574*, 511–515.
- (34) Aydin, G.; Koçak, O.; Gülcü, C.; Yavuz, I. Structural order and charge transfer in highly strained carbon nanobelts. *New J. Chem.* **2020**, *44*, 15769–15775.
- (35) Freixas, V. M.; Oldani, N.; Franklin-Mergarejo, R.; Tretiak, S.; Fernandez-Alberti, S. Electronic Energy Relaxation in a Photoexcited Fully Fused Edge-Sharing Carbon Nanobelt. *J. Phys. Chem. Lett.* **2020**, *11*, 4711–4719.
- (36) Ahn, D.-H.; Song, J.-W. Assessment of long-range corrected density functional theory on the absorption and vibrationally resolved fluorescence spectrum of carbon nanobelts. *J. Comput. Chem.* **2021**, *42*, 505–515.
- (37) Ehrenhauser, F. S. PAH and IUPAC Nomenclature. *Polycycl. Aromat. Comp.* **2015**, *35*, 161–176.
- (38) Saito, R.; Fujita, M.; Dresselhaus, G.; Dresselhaus, M. S. Electronic structure of chiral graphene tubules. *Applied Physics Letters* **1992**, *60*, 2204–2206.
- (39) Qian, L.; Xie, Y.; Zhang, S.; Zhang, J. Band Engineering of Carbon Nanotubes for Device Applications. *Matter* **2020**, *3*, 664–695.
- (40) Baydin, A.; Tay, F.; Fan, J.; Manjappa, M.; Gao, W.; Kono, J. Carbon Nanotube Devices for Quantum Technology. *Materials* **2022**, *15*.
- (41) Yang, F.; Wang, M.; Zhang, D.; Yang, J.; Zheng, M.; Li, Y. Chirality Pure Carbon Nanotubes: Growth, Sorting, and Characterization. *Chem. Rev.* **2020**, *120*, 2693–2758.
- (42) For the exceptional case of zigzag CNBs ($n, 0$) ($m = 0$), the enumeration is trivial since there is only one possible isomer with path code $[n]$.

- (43) Kelleher, J.; O'Sullivan, B. Generating All Partitions: A Comparison Of Two Encodings. *CoRR* **2009**, *abs/0909.2331*.
- (44) Hückel, E. Quantentheoretische Beiträge zum Benzolproblem. I. Die Elektronenkonfiguration des Benzols und werwandter Verbindungen. *Z. Phys.* **1931**, *70*, 204–286.
- (45) Hückel, E. Quantentheoretische Beiträge zum Bezołproblem. II. Quantentheorie der induzierten Polaritäten. *Z. Phys.* **1931**, *72*, 310–337.
- (46) Hückel, E. Quantentheoretische Beiträge zum Problem der aromatischen und ungesättigten Verbindungen. III. *Z. Phys.* **1932**, *72*, 628–648.
- (47) Hückel, E. Quantentheoretische Beiträge zum Bezołproblem. IV. Die freien Radikale der organischen Chemie. *Z. Phys.* **1933**, *83*, 632.
- (48) Fries, K. Über Bicyclische Verbindungen Und Ihren Vergleich MIT Dem Naphtalin. III. Mitteilung. *Justus Liebigs Ann. Chem.* **1927**, *454*, 121–324.
- (49) Fries, K.; Walter, R.; Schilling, K. Über Tricyclische Verbindungen, in Denen Naphtalin MIT Einem Heterocyclus Anelliert Ist. *Justus Liebigs Ann. Chem.* **1935**, *516*, 248–285.
- (50) Ciesielski, A.; Krygowski, T. M.; Cyrański, M. K. How to Find the Fries Structures for Benzenoid Hydrocarbons. *Symmetry* **2010**, *2*, 1390–1400.
- (51) Fowler, P. W.; Myrvold, W.; Bird, W. H. Counterexamples to a Proposed Algorithm for Fries Structures of Benzenoids. *J. Math. Chem.* **2012**, *50*, 2408–2426.
- (52) Wang, Y. Extension and Quantification of the Fries Rule and Its Connection to Aromaticity: Large-Scale Validation by Wave-Function-Based Resonance Analysis. *J. Chem. Inf. Model.* **2022**, *62*, 5136–5148.
- (53) Clar, E. *The Aromatic Sextet*; Wiley: New York, NY, 1972.
- (54) Solà, M. Forty Years of Clar's Aromatic π -Sextet Rule. *Front. Chem.* **2013**, *1*, 22.

- (55) Wang, Y. Quantitative Resonance Theory Based on the Clar Sextet Model. *J. Phys. Chem. A* **2022**, *126*, 164–176.
- (56) Pearson, R. G. Absolute electronegativity and hardness correlated with molecular orbital theory. *Proc. Natl. Acad. Sci. U.S.A.* **1986**, *83*, 8440–8441.
- (57) Pearson, R. G. Electronic spectra and chemical reactivity. *J. Am. Chem. Soc.* **1988**, *110*, 2092–2097.
- (58) Pearson, R. G. Absolute electronegativity and hardness: applications to organic chemistry. *J. Org. Chem.* **1989**, *54*, 1423–1430.
- (59) Geerlings, P.; De Proft, F.; Langenaeker, W. Conceptual Density Functional Theory. *Chem. Rev.* **2003**, *103*, 1793–1874.
- (60) Domingo, L. R.; Ríos-Gutiérrez, M.; Pérez, P. Applications of the Conceptual Density Functional Theory Indices to Organic Chemistry Reactivity. *Molecules* **2016**, *21*.
- (61) Chakraborty, D.; Chattaraj, P. K. Conceptual density functional theory based electronic structure principles. *Chem. Sci.* **2021**, *12*, 6264–6279.
- (62) Zhou, Z.; Parr, R. G. Activation hardness: new index for describing the orientation of electrophilic aromatic substitution. *J. Am. Chem. Soc.* **1990**, *112*, 5720–5724.
- (63) Aihara, J.-i. Correlation found between the HOMO–LUMO energy separation and the chemical reactivity at the most reactive site for isolated-pentagon isomers of fullerenes. *Phys. Chem. Chem. Phys.* **2000**, *2*, 3121–3125.
- (64) Oiwa, M.; Ryoshikagaku, S. *Elementary Quantum Chemistry*; Kagaku-Dojin: Kyoto, 1965.
- (65) Sato, T.; Tanaka, M.; Yamabe, T. Size-dependent HOMO-LUMO gap oscillation of carbon nanotube with a finite length. *Synth. Met.* **1999**, *103*, 2525–2526.

- (66) Bendikov, M.; Duong, H. M.; Starkey, K.; Houk, K. N.; Carter, E. A.; Wudl, F. Oligoacenes: Theoretical Prediction of Open-Shell Singlet Diradical Ground States. *J. Am. Chem. Soc.* **2004**, *126*, 7416–7417.
- (67) Esser, B. Theoretical analysis of [5.5.6]cyclacenes: electronic properties, strain energies and substituent effects. *Phys. Chem. Chem. Phys.* **2015**, *17*, 7366–7372.
- (68) Chen, Z.; Jiang, D.-e.; Lu, X.; Bettinger, H. F.; Dai, S.; Schleyer, P. v. R.; Houk, K. N. Open-Shell Singlet Character of Cyclacenes and Short Zigzag Nanotubes. *Org. Lett.* **2007**, *9*, 5449–5452.
- (69) Battaglia, S.; Faginas-Lago, N.; Andrae, D.; Evangelisti, S.; Leininger, T. Increasing Radical Character of Large [n]cyclacenes Unveiled by Wave Function Theory. *J. Phys. Chem. A* **2017**, *121*, 3746–3756.
- (70) Pérez-Guardiola, A.; Sandoval-Salinas, M. E.; Casanova, D.; San-Fabián, E.; Pérez-Jiménez, A. J.; Sancho-García, J. C. The role of topology in organic molecules: origin and comparison of the radical character in linear and cyclic oligoacenes and related oligomers. *Phys. Chem. Chem. Phys.* **2018**, *20*, 7112–7124.
- (71) Lakshman, M. K.; Kole, P. L.; Chaturvedi, S.; Saugier, J. H.; Yeh, H. J. C.; Glusker, J. P.; Carrell, H. L.; Katz, A. K.; Afshar, C. E.; Dashwood, W.-M.; Kenniston, G.; Baird, W. M. Methyl Group-Induced Helicity in 1,4-Dimethylbenzo[c]phenanthrene and Its Metabolites: Synthesis, Physical, and Biological Properties. *J. Am. Chem. Soc.* **2000**, *122*, 12629–12636.
- (72) Brulé, C.; Laali, K. K.; Okazaki, T.; Lakshman, M. K. Structure/Reactivity Relationships in the Benzo[c]phenanthrene Skeleton: Stable Ion and Electrophilic Substitution (Nitration, Bromination) Study of Substituted Analogues, Novel Carbocations and Substituted Derivatives. *J. Org. Chem.* **2007**, *72*, 3232–3241.

- (73) Sure, R.; Hansen, A.; Schwerdtfeger, P.; Grimme, S. Comprehensive theoretical study of all 1812 C₆₀ isomers. *Phys. Chem. Chem. Phys.* **2017**, *19*, 14296–14305.
- (74) Grimme, S.; Bannwarth, C.; Shushkov, P. A Robust and Accurate Tight-Binding Quantum Chemical Method for Structures, Vibrational Frequencies, and Noncovalent Interactions of Large Molecular Systems Parametrized for All spd-Block Elements ($Z = 1\text{--}86$). *J. Chem. Theory Comput.* **2017**, *13*, 1989–2009.
- (75) Bannwarth, C.; Ehlert, S.; Grimme, S. GFN2-xTB—An Accurate and Broadly Parametrized Self-Consistent Tight-Binding Quantum Chemical Method with Multipole Electrostatics and Density-Dependent Dispersion Contributions. *J. Chem. Theory Comput.* **2019**, *15*, 1652–1671.
- (76) Lee, C.; Yang, W.; Parr, R. G. Development of the Colle–Salvetti Correlation-Energy Formula Into a Functional of the Electron Density. *Phys. Rev. B* **1988**, *37*, 785–789.
- (77) Becke, A. D. Density-Functional Thermochemistry. III. The Role of Exact Exchange. *J. Chem. Phys.* **1993**, *98*, 5648–5652.
- (78) Grimme, S.; Ehrlich, S.; Goerigk, L. Effect of the damping function in dispersion corrected density functional theory. *J. Comput. Chem.* **2011**, *32*, 1456–1465.
- (79) Semiempirical Extended Tight-Binding Program Package. 2020; <https://github.com/grimme-lab/xtb/tree/v6.3.3>, (accessed March 29, 2023).
- (80) Frisch, M. J.; Trucks, G. W.; Schlegel, H. B.; Scuseria, G. E.; Robb, M. A.; Cheeseman, J. R.; Scalmani, G.; Barone, V.; Petersson, G. A.; Nakatsuji, H.; Li, X.; Caricato, M.; Marenich, A. V.; Bloino, J.; Janesko, B. G.; Gomperts, R.; Menennucci, B.; Hratchian, H. P.; Ortiz, J. V.; Izmaylov, A. F.; Sonnenberg, J. L.; Williams-Young, D.; Ding, F.; Lipparini, F.; Egidi, F.; Goings, J.; Peng, B.; Petrone, A.; Henderson, T.; Ranasinghe, D.; Zakrzewski, V. G.; Gao, J.; Rega, N.; Zheng, G.; Liang, W.;

Hada, M.; Ehara, M.; Toyota, K.; Fukuda, R.; Hasegawa, J.; Ishida, M.; Nakajima, T.; Honda, Y.; Kitao, O.; Nakai, H.; Vreven, T.; Throssell, K.; Montgomery, J. A.; Jr., Peralta, J. E.; Ogliaro, F.; Bearpark, M. J.; Heyd, J. J.; Brothers, E. N.; Kudin, K. N.; Staroverov, V. N.; Keith, T. A.; Kobayashi, R.; Normand, J.; Raghavachari, K.; Rendell, A. P.; Burant, J. C.; Iyengar, S. S.; Tomasi, J.; Cossi, M.; Millam, J. M.; Klene, M.; Adamo, C.; Cammi, R.; Ochterski, J. W.; Martin, R. L.; Morokuma, K.; Farkas, O.; Foresman, J. B.; Fox, D. J. Gaussian 16, Revision B.01. 2017.

- (81) Wang, Y. The EzReson program. 25 Jun. 2020; <https://github.com/yangwangmadrid/EzReson>.
- (82) Wang, Y. Superposition of Waves or Densities: Which is the Nature of Chemical Resonance? *J. Comput. Chem.* **2021**, *42*, 412–417.
- (83) Wang, Y. A Reliable and Efficient Resonance Theory Based on Analysis of DFT Wave Functions. *Phys. Chem. Chem. Phys.* **2021**, *23*, 2331–2348.
- (84) The MathWorks Inc., MATLAB version: 9.14.0.2206163 (R2023a). 2023; <https://www.mathworks.com>.
- (85) Jmol: an open-source Java viewer for chemical structures in 3D (version 14.30.2). 2015; <http://www.jmol.org/>.

Graphical TOC Entry

